

# HiSST: 4th International Conference on High-Speed Vehicle Science Technology





# Optimized Multi-Interceptor Deployment Strategy for Hypersonic Targets Using Predictive Reachability Analysis

Yuchen. HAN<sup>1, 2</sup>, Ming. YANG<sup>1, 2</sup>, Ping. MA<sup>1, 2</sup>, Tao. CHAO<sup>1, 2</sup>

#### **Abstract**

This study proposes a multi-interceptor deployment strategy against high-speed maneuvering targets in atmospheric flight, leveraging predictive footprint analysis to optimize defensive coverage. An analytical model is developed to determine interceptor footprints based on maneuverability constraints and curve-fitting techniques, allowing rapid generation of engagement boundaries from specified launch points and predicted impact locations. By integrating this model with target footprint prediction, the interception problem is reformulated as a coverage optimization problem. A dedicated algorithm is designed to compute minimal-interceptor deployments that maximize coverage of the target's potential trajectories. Numerical simulations demonstrate the method's ability to achieve effective interception with reduced resource allocation, confirming its operational feasibility against high-speed maneuvering threats.

**Keywords**: Hypersonic Targets, Predictive Reachability Analysis, Multi-Interceptor Deployment Strategy, Optimization Algorithm.

#### **Nomenclature**

Latin

a – Major axis of the footprint fitted ellipse

*b* – Minor axis of the footprint fitted ellipse

d-Maximum range in the latitude-longitude plane

*g* – Standard gravitational acceleration constant

m-Mass

V - Velocity

BL - The terminal coordinate of target

D - Drag force

*K* − Lift-to-drag ratio

M – Number of predicted trajectories

*N* – Number of interceptors

 $R_t$  – Geocentric distance

Greek

 $\alpha$  – Angle of attack

 $\alpha_1$  – Commanded angle of attack in the first-

stage boost phase

 $\alpha_2$  – Commanded angle of attack in the

second-stage boost phase

 $\alpha_k$  – Absolute value of the maximum angle of attack in the first second-state boost phase;

 $\alpha_m$  – Absolute value of the maximum angle of attack in the first second-state boost phase;

 $\delta_c$  – Crossrange angle

 $\lambda$  – Longitude

 $\phi$  – Latitude

 $(\phi_0, \lambda_0)$  – Glide point coordinate of interceptor

 $(\phi_1, \lambda_1)$  – Maximum downrange endpoint

coordinate of interceptor

 $(\phi_2, \lambda_2)$  – Left maximum crossrange endpoint

coordinate of interceptor

 $(\phi_3, \lambda_3)$  – Right maximum crossrange endpoint coordinate of interceptor

 $(\phi_C, \lambda_C)$  – Center point coordinate of the

footprint fitted ellipse

 $\theta$  – Flight path angle

 $\sigma$  – Heading azimuth angle of the HBGV

 $\nu$  – Bank angle

HiSST-2025-XXXX Paper Title Page | 1 Copyright © 2025 by author(s)

<sup>&</sup>lt;sup>1</sup> Control and Simulation Center, Harbin Institute of Technology, Harbin, China.

<sup>&</sup>lt;sup>2</sup> National Key Laboratory of Modeling and Simulation for Complex Systems, Harbin Institute of Technology, Harbin, China.

 $\Phi$  – Angle between the major axis of the ellipse and the horizontal axis of latitude Subscripts f – Terminal point

i – Index of HBGVj – Index of interceptork – Index of scheme

#### 1. Introduction

Hypersonic vehicles are widely regarded as game-changing technologies with the potential to "reshape the rules of future warfare" [1], and have thus become a central focus of research among major global powers. Based on their propulsion systems, hypersonic vehicles can be broadly classified into two main categories: hypersonic boost-glide vehicles (HBGVs) and hypersonic cruise vehicles (HCVs) [2]. HBGVs use booster rockets to attain near-space or ex-atmospheric insertion before re-entering the atmosphere for sustained unpowered gliding. In contrast, HCVs employ scramjet propulsion to maintain powered hypersonic cruise within near-space environments. Compared to traditional ballistic missiles, both types of hypersonic systems exhibit not only extreme velocities—with HBGVs reaching Mach 10–15 during glide and HCVs cruising at Mach 5–6 [3] but also enhanced agility, unpredictable trajectories, and superior maneuverability. These capabilities pose unprecedented challenges to modern defense systems.

The principal challenges in defending against hypersonic targets originate from two critical factors. First, HBGVs possess extended operational ranges that surpass the detection capabilities of current space-based early warning systems. At the same time, ground-based radars are constrained by the Earth's curvature, further limiting their observational reach. Moreover, the low-altitude glide phase of HBGVs substantially shortens the effective observation windows of ground radars. This issue is exacerbated by their erratic trajectory maneuvers, which severely hinder accurate tracking and reliable trajectory prediction. Second, these targets sustain atmospheric flight velocities that match or exceed those of interceptors, all while exhibiting significant lateral maneuverability. This combination imposes rigorous demands on the decision-making processes and guidance methodologies of defense systems during interception.

In response to the first challenge, nations are actively developing advanced architectures for early warning and detection systems. Concerning the second challenge, the unpredictable, high-amplitude maneuvers of hypersonic vehicles pose a more severe threat than high speed alone. Experts have noted several common misconceptions in hypersonic defense, including an overemphasis on velocity as the principal obstacle to interception. While the high velocities of HBGVs indeed challenge sustained radar tracking, conventional ballistic trajectories—if predictable—would allow accurate forecasting and successful interception. The core difficulty lies in the unpredictable "skip-glide" vertical motion and lateral evasive maneuvers of HBGVs, which collectively undermine the effectiveness of traditional interception tactics.

To address these challenges, HBGVs can be abstracted conceptually as high-speed maneuvering targets within the atmosphere for the purpose of interception analysis. By formulating effective multi-interceptor deployment strategies based on pre-launch observational data, along with implementing precise mid-course guidance adjustments, the likelihood of successful interception by at least one interceptor can be substantially increased.

Existing literature predominantly focuses on interception decision-making design for kinetic kill vehicles, with limited research on pre-launch interceptor deployment strategies. Reference [4] developed a 0-1 integer programming model for interception decisions that incorporates radar guidance capabilities and constraints on interceptor quantity and location. Reference [5] analyzed endgame interception processes and proposed a conical footprint model in which the generatrix represents the maximum acceleration paths perpendicular to the interceptor's velocity vector, expressed using velocity azimuth and elevation angles. Through spatial geometric analysis, explicit expressions were derived for both interceptor capture domains and target escape domains, leading to an engagement domain model incorporating energy constraints. Reference [6] addressed cooperative multi-target interception using deep reinforcement learning, first evaluating interceptor capability before transforming the many-to-many interception problem into multiple many-to-one scenarios via target allocation, ultimately designing a neural network for cooperative decision-making with position-biased proportional navigation. Reference [7] derived interception probability density functions based on reachable set analysis, integrating these to calculate single and joint interception probabilities. Their approach

balanced target cluster interception probability against fuel consumption through a decision treeoptimized performance metric preserving maneuverability reserves. References [8,9] employed conventional simulation to generate engagement domain scatter plots, developing analytical equations via particle swarm optimization for parameter fitting. These parameters served as inputs for backpropagation neural networks to enable rapid engagement domain calculation, supporting interception decisions. Under bounded maneuverability assumptions, Reference [10] designed bangbang guidance laws in 2D planes, proposing both preset and adaptive cooperative strategies to ensure target coverage by combined interceptor acceleration footprints, Extending this work, Reference [11] introduced virtual aim points to bias acceleration footprints, reducing 3D cooperative problems to 2D circular coverage scenarios. Following similar coverage principles, reference [12] designed 2D cooperative quidance laws under nonlinear engagement geometry, developing a multi-interceptor allocation algorithm for target escape domains. However, their guidance law's dependence on target acceleration and velocity lead angle data - often unavailable in real engagements - compromises interception performance. Current research on multi-interceptor engagement strategies exhibits two primary limitations; first, most approaches operate under the assumption of known or bounded target maneuver acceleration magnitudes, failing to fully leverage estimated target information for trajectory prediction or maneuver capability modeling; second, existing solutions predominantly rely on interceptor communication networks, resulting in poor robustness and incompatibility with communication-denied complex battlefield environments.

HBGVs present unique challenges during their glide phase, characterized by extreme velocities, high lift-to-drag ratios, and extensive lateral maneuverability combined with skip-glide capabilities, all of which significantly complicate accurate trajectory prediction. A viable solution involves predicting HBGV footprints using historical and real-time detection data from space-based platforms and ground-based radars. Although sensor inaccuracies and HBGV maneuver uncertainties may yield relatively large prediction regions, appropriately designed multi-interceptor strategies can achieve comprehensive coverage of these domains using interceptors with inferior maneuverability compared to HBGVs, thereby ensuring a high probability of successful interception by at least one interceptor.

Regarding footprint prediction, reference [13] proposed an HBGV prediction method based on equilibrium glide assumptions and optimal flight criteria [14], demonstrating superior accuracy and computational efficiency compared to conventional numerical prediction and constant bank angle methods [15]. Building upon this rapid prediction framework, this paper develops a novel communication-independent multi-interceptor decision-making methodology to enhance interception probability.

### 2. Rapid Prediction of Attacker's Footprint

The prediction of HBGV footprint comprises two fundamental components: maximum downrange and crossrange capability prediction. This section provides a concise exposition of the predictive methodology delineated in reference [14], which serves as the foundational input for subsequent cooperative interception decision-making algorithms.

Assuming that the estimated value of the current state of HBGV is obtained through the filtering and estimation of the previous observational data, which includes the position vector, velocity vector, and maximum lift-to-drag ratio in the geocentric system. The following introduces a rapid prediction method for the footprint of the attacking projectile based on the estimated values.

#### 2.1. Maximum Downrange Prediction

Under the equilibrium glide assumption, the rate of flight path angle and the flight path angle itself are approximately zero (i.e.  $\dot{\theta} \approx 0$ ,  $\theta \approx 0$ ). This is commonly used in the footprint prediction of HBGV. On one hand, it ensures that the state variables possess favorable analytical properties; on the other hand, it can approximate the optimal solution for minimum load factor and maximum range. Based on the assumptions of equilibrium glide, zero bank angle ( $\upsilon=0$ ), and maximum lift-to-drag ratio ( $K_{\rm max}$ ), while neglecting Earth's rotation effects, the 3-DOF equations of motion for HBGV are derived as follows:

$$\begin{cases} \dot{R}_{t} = v \sin \theta, \\ \dot{\lambda} = \frac{v \cos \theta \sin \sigma}{R_{t} \cos \phi}, \\ \dot{\phi} = \frac{v \cos \theta \cos \sigma}{R_{t}}, \\ \dot{v} = \frac{\left(gR_{t} - v^{2}\right) \cos \theta}{R_{t} K_{\text{max}}} - g \sin \theta, \\ \dot{\theta} = 0, \\ \dot{\sigma} = \frac{v \tan \phi \cos \theta \sin \sigma}{R_{t}}, \end{cases}$$
(1)

In the equations,  $R_t$ ,  $\lambda$ ,  $\phi$ ,  $\nu$ ,  $\theta$  and  $\sigma$  represent the geocentric distance, longitude, geocentric latitude, velocity, flight path angle, and heading azimuth angle of the HBGV, respectively. Given the terminal velocity lower limit  $\nu_f$  of the HBGV, the initial values are selected as the current state estimates of the vehicle. By numerically integrating Eq. (1), the maximum-range trajectory can be obtained.

#### 2.2. Maximum Crossrange Prediction

The optimal bank angle is computed as [16]

$$\upsilon = \frac{1}{2}e^{\frac{K_{\text{max}}}{5}}\arctan\left(\frac{\cos\delta_c}{\tan(\sigma - \sigma_0)}\right)$$
 (2)

In the equation,  $\delta_c$  denotes the crossrange angle. Under the assumptions of equilibrium glide and maximum lift-to-drag ratio glide, the drag force can be expressed as:

$$D = \frac{m(gR_t - v^2)\cos\theta}{R_t K_{\text{max}}\cos\upsilon}$$
 (3)

The maximum crossrange differential equation for the HBGV is obtained by combining Eq. (2) and Eq. (3) as:

$$\begin{cases} \dot{R}_{t} = v \sin \theta, \\ \dot{\lambda} = \frac{v \cos \theta \sin \sigma}{R_{t} \cos \phi}, \\ \dot{\phi} = \frac{v \cos \theta \cos \sigma}{R_{t}}, \\ \dot{v} = -\frac{(gR_{t} - v^{2}) \cos \theta}{R_{t} K_{\text{max}} \cos v} - g \sin \theta, \\ \dot{\theta} = 0, \\ \dot{\sigma} = -\left(\frac{g}{v} - \frac{v}{R_{t}}\right) \cos \theta \tan v + \frac{v \tan \phi \cos \theta \sin \sigma}{R_{t}}. \end{cases}$$

$$(4)$$

By numerically integrating Eq. (4) with the same initial values and terminal conditions as those used for the maximum-range trajectory, the maximum crossrange trajectory can be obtained.

A trajectory point from the HBGV glide phase is selected as the prediction initial point. The footprint of trajectories obtained using the maximum-range and maximum-crossrange prediction methods is shown in Fig. 1. The figure displays multiple maximum-crossrange trajectories (not just one) because different saturation limits ( $|v_{max}|=10^{\circ}$ , 20°, ..., 60°) were applied to the bank angle Eq. (2) during

numerical integration of Eq. (4), resulting in 6 trajectories on each side (left and right). Furthermore, the extensive footprint in Fig. 1 demonstrates the HBGV's strong lateral maneuvering capability, making complete coverage of its footprint challenging. However, for the subsequent multi-interceptor deployment method designment, the termination conditions for footprint trajectory prediction will incorporate not only terminal velocity constraints but also time-of-prediction requirements.

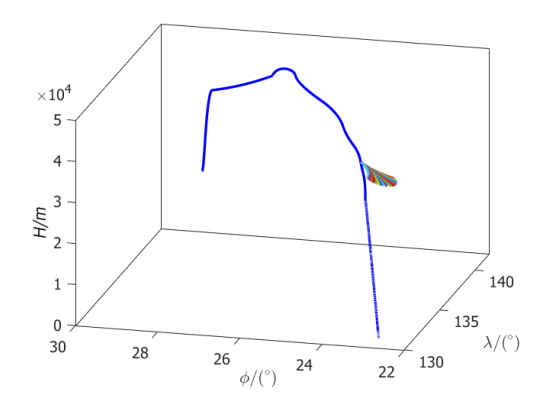


Fig 1. Footprint of HBGV

# 3. Model of Interceptor Maneuverability Footprint

The interceptor's maneuverable footprint is determined by its maneuvering capability and will directly influence subsequent engagement decision-making outcomes. Therefore, this section will conduct a detailed analysis of the interceptor's maneuvering characteristics.

The selected interceptor configuration consists of a two-stage booster and a kinetic kill vehicle. For initial guidance, a programmed guidance scheme is adopted, with pitch angle commands designed for both the first and second stage boosters as follows:

$$\alpha(t) = \begin{cases} \alpha_1(t), & 0 \leq t < t_1, \\ \alpha_2(t), & t_1 \leq t < t_2, \\ 0, & \text{else.} \end{cases}$$
 (5)

The equation parameters are defined as follows:  $t_1$  represents the shutdown time of the first-stage booster,  $\alpha_1$  denotes the programmed angle-of-attack command to be designed for the first-stage booster,  $t_2$  indicates the shutdown time of the second-stage booster, and  $\alpha_2$  stands for the programmed angle-of-attack command to be designed for the second-stage booster.

The design of the angle-of-attack variation profile follows the methodology presented in reference [17], where is

$$\alpha_1(t) = 4\alpha_k \frac{t(t - t_1)}{t_2^2} \tag{6}$$

$$\alpha_2(t) = 4\alpha_m \exp(-a(t - t_1))(1 - \exp(-a(t - t_1)))$$
 (7)

Where a is a positive constant, and  $\alpha_k$ ,  $\alpha_m$  represent the absolute value of the maximum angle of attack.

According to literature research, the glide altitude of HBGV typically ranges between 20–60 km[18], with most cases falling within 20–40 km [19], to fully utilize aerodynamic forces for skip-gliding and significant lateral maneuvers.

For the high-altitude interception during the terminal glide phase discussed in this paper, considering the interceptor's axisymmetric structure and the fact that mid-course guidance relies on aerodynamic forces to provide the required control, its lateral maneuvering is reflected in the commanded sideslip angle  $\beta c$ . Traditional maximum crossrange calculations for HBGV often assume a

constant bank angle, yielding highly accurate results. Inspired by this, the present study employs a constant commanded sideslip angle to characterize the interceptor's lateral maneuvering capability. Furthermore, without specifying a particular mid-course guidance law, using a constant commanded sideslip angle to derive the interceptor's lateral maneuvering capability through numerical simulation is reasonable.

Two key points require attention:

Since the standard trajectory becomes unguided after the boost phase, with a commanded angle of attack  $\alpha_c=0$ , the interceptor's altitude decreases faster under a constant commanded sideslip angle  $\beta_c=0$  compared to an unguided trajectory. However, this can be mitigated in actual mid-course guidance through proper guidance command generation. Therefore, for the interceptor's footprint analysis, altitude variations are neglected, and only the maximum range and crossrange in the latitude-longitude 2D plane are considered.

Atmospheric density varies with altitude, affecting the interceptor's maneuvering capability and, consequently, its footprint.

To address the second point, this section employs a fitting method for the characteristic parameters of the interceptor's footprint at different altitudes. By selecting different  $\alpha_m$  values (each corresponding to a distinct standard trajectory and thus a different interception altitude) and applying a series of constant commanded sideslip angles, simulations yield the interceptor's footprint in the latitude-longitude plane, as shown in Fig 2. The results indicate that the 2D footprint boundary approximates a sector, with smaller am values (i.e., less trajectory depression) leading to larger sector-like regions.

To further investigate the boundary characteristics of the interceptor's footprint, Fig 3 illustrates its general footprint. Here,  $(\phi_i, \lambda_i)$ , where i = 0, 1, 2, 3, represent the interceptor's glide point, maximum downrange endpoint, and left/right maximum crossrange endpoints, respectively. The distance d denotes the maximum range in the latitude-longitude plane, measured in degrees (°).

By referring to the fitting of the boundary of the HBGV footprint in reference [15], this section defines the boundary of the interceptor's footprint as an ellipse. The minor axis of this ellipse is the line connecting points  $(\phi_2, \lambda_2)$  and  $(\phi_3, \lambda_3)$ , and the semi-major axis is the line connecting point  $(\phi_1, \lambda_1)$  to the center of the minor axis.

Denote the center of the ellipse as  $(\phi_c,\lambda_c)$  , where the calculation formulas of the center coordinates are:

$$\phi_c = \frac{(\phi_2 + \phi_3)}{2}, \quad \lambda_c = \frac{(\lambda_2 + \lambda_3)}{2}$$
 (8)

Then, the semi-major axis a and semi-minor axis b of the ellipse are calculated by the following formulas respectively:

$$a = \sqrt{(\phi_c - \phi_1)^2 + (\lambda_c - \lambda_1)^2}$$
(9)

$$b = \sqrt{(\phi_c - \phi_2)^2 + (\lambda_c - \lambda_2)^2}$$
 (10)

Let  $\Phi$  represent the angle between the major axis of the ellipse and the horizontal axis of latitude; its calculation formula is:

$$\Phi = \arctan\left[\left(\phi_{1} - \phi_{c}\right) / \left(\lambda_{1} - \lambda_{c}\right)\right]$$
(11)

Thus, the equation of the ellipse is expressed as follows:

$$\frac{\left(\left(\phi - \phi_{c}\right)\cos\Phi + \left(\lambda - \lambda_{c}\right)\sin\Phi\right)^{2}}{a^{2}} + \frac{\left(-\left(\phi - \phi_{c}\right)\sin\Phi + \left(\lambda - \lambda_{c}\right)\cos\Phi\right)^{2}}{b^{2}} = 1 \tag{12}$$

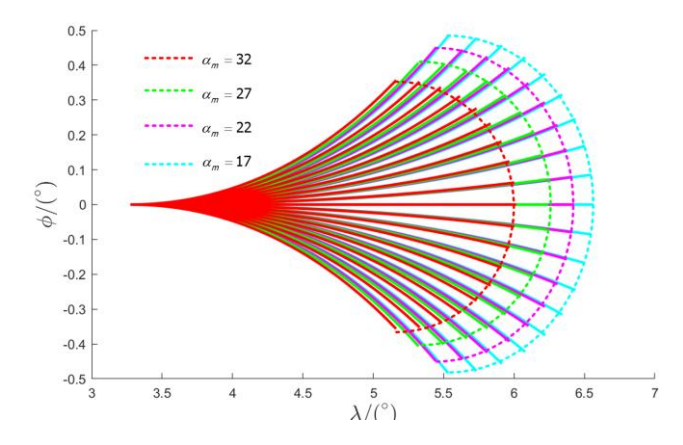


Fig 2. Footprint of interceptor with different values of  $\,\alpha_{\it m}$ 

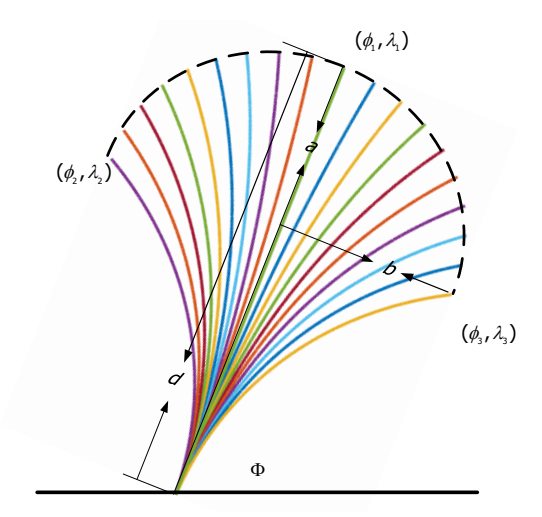


Fig 3. General footprint of interceptor

Numerically simulating the footprint of interceptors each time demands high computing power and consumes excessive time, which prolongs the interception decision-making process. This not only significantly compresses the launch preparation time for interceptors but also increases the likelihood of missing the optimal interception window. Therefore, based on the aforementioned modeling of the footprint, an analytical method is employed to achieve rapid calculation of the interceptor's footprint.

**Table 1.**Characteristic parameters values of the footprint of interceptor with different values of  $\alpha_m$ 

program angle $\alpha_{\scriptscriptstyle m}$	interception altitude H   km	semi- major axis a / °	semi- minor axis b/°	maximum downrange d / °
17	55.80	0.5494	0.1732	1.8174
20	47.65	0.5280	0.1612	1.7483
22	42.23	0.5109	0.1518	1.6931
25	34.12	0.4815	0.1373	1.6022
27	28.75	0.4604	0.1264	1.5332
30	20.76	0.4269	0.1098	1.4227
32	15.48	0.4003	0.0985	1.3403
35	7.66	0.3612	0.0810	1.2093

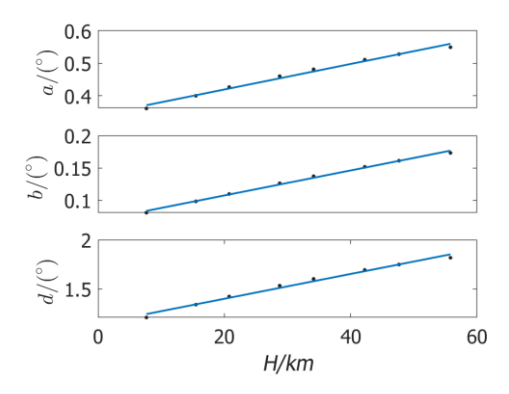


Fig 4. Curves of boundary characteristic parameters of interceptor footprint with different altitudes

As can be seen from Fig. 4, there is a basically linear relationship between the two. Then, by fitting the relationship between the characteristic parameters and the interception altitude using a linear function, the boundary of the footprint of the interceptor can be quickly calculated according to the required interception altitude. The fitting functions for each characteristic parameter are as follows:

$$a = 0.003923H + 0.341 \tag{13}$$

$$b = 0.001929H + 0.06901 \tag{14}$$

$$d = 0.01263H + 1.147 \tag{15}$$

To determine the elliptic function Eq.(12) for the boundary of the footprint, in addition to the above mentioned characteristic parameters, it is also necessary to determine the center point of the ellipse  $(\phi_c, \lambda_c)$  and the end - point of the maximum downrange  $(\phi_1, \lambda_1)$ . When the latitude and longitude coordinates of the predicted impact point  $(\phi_p, \lambda_p)$  are given, through geometric analysis, the coordinates of the center point of the ellipse and the end point of the maximum downrange can be calculated according to the following steps:

In the latitude - longitude plane, the straight line determined by the glide point  $(\phi_0, \lambda_0)$  and the predicted impact point  $(\phi_0, \lambda_0)$  is

$$\lambda - \lambda_0 = \frac{\lambda_\rho - \lambda_0}{\phi_\rho - \phi_0} (\phi - \phi_0)$$
 (16)

The endpoint of the maximum downrange satisfies the above equation and is at a distance d from the glide point, thus determining the following system of equations:

$$\begin{cases} \lambda_{1} - \lambda_{0} = \frac{\lambda_{p} - \lambda_{0}}{\phi_{p} - \phi_{0}} (\phi_{1} - \phi_{0}) \\ (\lambda_{1} - \lambda_{0})^{2} + (\phi_{1} - \phi_{0})^{2} = d^{2} \end{cases}$$
 (17)

Solving the system of equations, the endpoint of the maximum range is obtained as

$$\begin{cases}
\phi_{1} = \phi_{0} + \frac{d}{\sqrt{1 + \left[ (\lambda_{\rho} - \lambda_{0}) / (\phi_{\rho} - \phi_{0}) \right]^{2}}}, & \phi_{\rho} \geqslant \phi_{0}, \\
\phi_{1} = \phi_{0} - \frac{d}{\sqrt{1 + \left[ (\lambda_{\rho} - \lambda_{0}) / (\phi_{\rho} - \phi_{0}) \right]^{2}}}, & \phi_{\rho} < \phi_{0}, \\
\lambda_{1} = \lambda_{0} + d, & \phi_{\rho} = \phi_{0} \text{and } \lambda_{\rho} \geqslant \lambda_{0}, \\
\lambda_{1} = \lambda_{0} - d, & \phi_{\rho} = \phi_{0} \text{and } \lambda_{\rho} < \lambda_{0}, \\
\lambda_{1} = \lambda_{0} + \frac{\lambda_{\rho} - \lambda_{0}}{\phi_{\rho} - \phi_{0}} (\phi_{1} - \phi_{0}), & \text{Other cases.} 
\end{cases} \tag{18}$$

Then, the center point of the ellipse is determined as

$$\begin{cases}
\phi_c = \phi_0 + \frac{d - a}{d} (\phi_1 - \phi_0), \\
\lambda_c = \lambda_0 + \frac{d - a}{d} (\lambda_1 - \lambda_0).
\end{cases}$$
(19)

Therefore, each time the glide point of the interceptor and the predicted impact point are given, based on Eq. (13) to Eq. (19) and Eq. (11), the function Eq. (12) for the boundary of the footprint of the interceptor at the altitude where the predicted impact point is located can be quickly solved.

## 4. Multi Interceptor Decision-making Method

Section 1 adopts the balanced glide assumption for the trajectory footprint prediction of HBGV, so it can be considered that the predicted trajectory terminal altitudes differ slightly. Combined with the analytical model of the interceptor's footprint established in the latitude-longitude plane in Section 2, this section transforms the interception decision-making problem into an offensive and defensive footprint coverage optimization problem within the latitude-longitude plane, and solves the multi-interceptor deployment strategy through designing an optimization algorithm.

Suppose that M HBGVS' trajectories are obtained from the footprint prediction in Section 1, and the terminal coordinate of the i-th trajectory is  $BL_{fi} = (\phi_{fi}, \lambda_{fi})$ , where  $i = 1, 2, \cdots, M$ . Calculate the average value of the predicted trajectory terminal altitudes  $\overline{H}_f$ , and substitute it into Eq. (13) to (15) to determine the characteristic parameters a, b, and d of the interceptor's footprint.

Given the interceptor glide point  $BL_0 = (\phi_0, \lambda_0)$  and the number of interceptor N, the purpose of footprint coverage optimization is to determine the launch azimuth angle  $A_j$  of each interceptor (where  $j=1,2,\cdots,N$ ,) and  $(A_j$  is determined by the selected predicted trajectory terminal  $BL_{fi}$ ), so as to maximize the number of predicted HBGV trajectory terminals covered by the interceptor.

To solve this optimization problem, first analyze the j-th single interceptor. Select the predicted impact point of the j-th interceptor as the terminal of the  $k_j$ -th HBGV trajectory (where  $k_j=1,2,\cdots,M$ ) with coordinate  $BL_{f_{k_j}}$ . Determine the characteristic parameters of the footprint boundary  $T_j=(\phi_{j,1},\lambda_{j,1},\phi_{j,c},\lambda_{j,c})$  according to Eq. (18) and Eq.(19), and substitute  $T_j$  into the left side of Eq. (12) to obtain the footprint boundary function:

$$F_{j,k_j}(\phi,\lambda) = \frac{\left((\phi - \phi_{j,c})\cos\Phi_j + (\lambda - \lambda_{j,c})\sin\Phi_j\right)^2}{a^2} + \frac{\left(-(\phi - \phi_{j,c})\sin\Phi_j + (\lambda - \lambda_{j,c})\cos\Phi_j\right)^2}{b^2}$$
(20)

When a predicted trajectory terminal  $BL_j = (\phi_j, \lambda_j)$ ,  $(i = 1, 2, \dots, M)$  is surrounded by the footprint boundary of interceptor j,  $F_{j,k_j}(\phi_l, \lambda_l) \le 1$ . When the terminal is outside the boundary,  $F_{j,k_j}(\phi_l, \lambda_l) \ge 1$ . Therefore, a more precise optimization objective is: determine distinct predicted impact points for each interceptor, so that the sum of the F-function values of N interceptors is minimized, so as to ensure that the joint footprint covers as many predicted trajectory terminals as possible. It is expressed by the following mathematical formulas:

$$J = \sum_{j=1}^{N} \sum_{i=1}^{M} F_{j,k_{j}}(\phi_{i}, \lambda_{i}),$$

$$(k_{1}, k_{2}, \dots, k_{N}) = \operatorname{argmin} J,$$
s.t.  $k_{p} \neq k_{q}; k_{p}, k_{q} = 1, 2, \dots, M; p, q = 1, 2, \dots, N.$ 
(21)

However, it should be noted that the optimization problem obtained by the above modeling, i.e., Eq. (21), does not consider the problem of repeated coverage. As a result, the coverage areas of each

interceptor in the optimization result are dense and have a large overlapping area, and the maneuverable footprint of each interceptor cannot be fully utilized. To solve this problem, Eq. (22) is used to replace the footprint boundary function:

$$G_{j,k_{j}}(\phi_{j},\lambda_{j}) = \begin{cases} 1, & F_{j,k_{j}}(\phi,\lambda) \le 1\\ 0, & F_{j,k_{j}}(\phi,\lambda) > 1 \end{cases}$$
 (22)

That is, binary representation is used to indicate the situation where the footprint of the interceptor covers the trajectory terminal. The value of the coverage indicator function G is 1 if covered, else is 0. Thus, Eq. (21) is transformed into the optimization problem shown in Eq. (23)

$$J = \sum_{j=1}^{N} \sum_{i=1}^{M} G_{j,k_{j}}(\phi_{i}, \lambda_{i}),$$

$$(k_{1}, k_{2}, \dots, k_{N}) = \operatorname{argmax} J,$$
s.t.  $k_{p} \neq k_{q}; k_{p}, k_{q} = 1, 2, \dots, M;$ 

$$p, q = 1, 2, \dots, N;$$

$$\sum_{j=1}^{N} G_{j,k_{j}}(\phi_{i}, \lambda_{i}) = 1$$
(23)

Compared with Eq. (21), Eq. (23) has two modifications. On one hand, within the performance index, the footprint boundary function is changed from Eq. (20) to Eq.(22), and the coverage of predicted trajectory terminals is represented in a clearer binary form. On the other hand, it restricts the repeated inclusion of the index function after any trajectory terminal  $BL_{fi}=(\phi_{fi},\lambda_{fi})$  is covered. If the p-th interceptor covers  $BL_{fi}=(\phi_{fi},\lambda_{fi})$  and this coverage is counted into the performance index function (i.e., J=J+1), then the re-coverage of  $BL_{fi}$  by the q-th interceptor will not be counted into the performance index function (i.e., J=J+0). This enables each interceptor to make full use of its own maneuverable footprint to cover the maximum number of predicted trajectory terminals.

Algorithm 1 presents the pseudocode of the footprint coverage optimization algorithm. Since the number of predicted trajectories M is limited, and the solution based on the analytical formula for the interceptors' footprint boundary derived in Section 2 greatly reduces the computational load, under the constraints that the predicted impact points assigned to each interceptor are different and the repeated coverage of predicted trajectory terminals is not counted into the performance index, the combination matrix—can be used to enumerate all possible selections of predicted impact points for the N interceptors, allowing for rapid traversal optimization. A record matrix Record is introduced in the pseudocode to track the coverage status of each predicted trajectory terminal. Only when it is determined that a certain trajectory terminal is not covered by the footprint of any interceptor can the performance index J be further updated and calculated.

# Algorithm 1 Pseudocode of footprint coverage optimization algorithm

In: the number of interceptors N, the predicted trajectory endpoints  $BL_{f1}$ ,  $BL_{f2}$ , ...,  $BL_{fM}$ 

Out: The predicted impact point allocation scheme PIP

1. Initialization: J=0, Optimal Performance Index Value  $J_{max}=0$ , PIP=[], Combination Matrix

$$Dir = C_M^N \times N$$

- 2. For  $k = 1: C_M^N$
- 3. Record = zeros(N, M);
- 4. For j = 1: N
- 5. If Record(:,i) = zeros(N,1)
- 6.  $J = J + G_{j,k_j}(\phi_j,\lambda_j);$

```
Record(j, i) = G_{j,k_i}(\phi_i,\lambda_i);
 7.
 8.
                   End
 9.
             end
10.
             If J > J_{\text{max}}
11.
                   J_{\text{max}} = J;
                   PIP = Dir(k,:)
12.
13.
14.
             Record = zeros(N, M);
15.
```

The optimization algorithm mentioned above takes the number of interceptors N is a given input. However, in practical scenarios, the maximum number of interceptors  $N_{\text{max}}$  is usually known, and the goal is to use the minimum number of interceptors while maximizing the coverage of predicted ballistic trajectories through interception decision-making. Therefore, the optimization problem is further transformed into:

$$\min_{N \in C} \sum_{j=1}^{N} \sum_{i=1}^{M} G_{j,k_{j}}(\phi_{i}, \lambda_{i})$$
s.t.  $k_{p} \neq k_{q}; k_{p}, k_{q} = 1, 2, ..., M;$ 

$$p, q = 1, 2, ..., N;$$

$$C = \{1, 2, ..., N_{\text{max}}\};$$

$$\sum_{j=1}^{N} G_{j,k_{j}}(\phi_{i}, \lambda_{j}) = 1.$$
(24)

The optimization problem presented in Eq. (24) incorporates an additional optimization objective of minimizing the number of interceptors, compared with Eq. (23). Therefore, based on the optimization algorithm outlined in Algorithm 1, an outer loop—where the number of interceptors ranges from 1 to  $N_{\rm max}$  is added. This transforms the original problem into  $N_{\rm max}$  distinct optimization subproblems, each with a fixed and specific number of interceptors. By storing the results of each optimization run, comparative analysis enables the acquisition of three key outputs:

 ${\it J}$  the maximum number of predicted ballistic trajectory endpoints that can be covered;  ${\it N}_{\rm min}$ : the minimum number of interceptors required to achieve this maximum coverage;  ${\it PIP}$ : the distribution of predicted impact points allocated to each interceptor.

#### 5. Simulation Validation

Set the current position of the HBGV as  $(25.7722^{\circ},136.818^{\circ},49.491\,\mathrm{km})$ , with a velocity of  $3000\,\mathrm{m/s}$ ; the velocity inclination angle and track yaw angle are  $\theta=-0.1^{\circ}$  and  $\sigma=-242.5^{\circ}$ , respectively. The estimated value of the maximum lift-to-drag ratio is  $K_{\mathrm{max}}=3$  Based on the current state, a backward prediction is performed for a time interval of  $\Delta T_t=100s$  Using the HBGV trajectory footprint prediction method described in Section 1, the predicted footprint trajectories are obtained as shown in Fig 5.

For the mentioned generated predicted trajectories, the number  $M\!=\!13$ . To facilitate the algorithm's solution output, the endpoint of the trajectory with the maximum longitudinal range is labeled as 1; the endpoints of the adjacent trajectories to its left and right are labeled as 2 and 3, respectively; and the remaining trajectory endpoints are labeled in sequence. Given the maximum number of interceptors  $N_{\text{max}}=5$ , the strike point of the HBGV is selected as the glide point of the interceptors.

Through the optimization of the problem formulated in Eq. (24), the following results are obtained:

the maximum number of predicted trajectory endpoints that can be covered J=13, the minimum number of interceptors required  $N_{\rm min}=3$ , and the Predicted Impact Point allocation for each interceptor, which is PIP=(1,11,13).

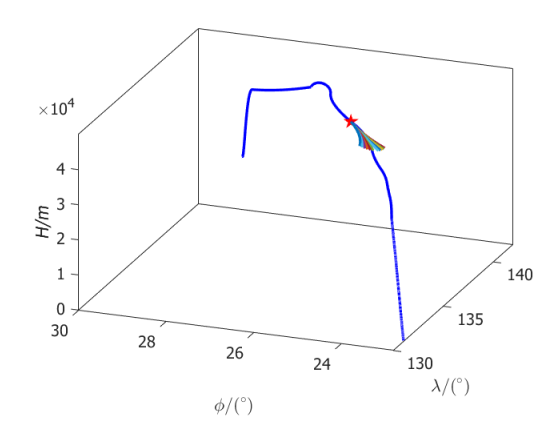


Fig 5. Simulation results of HBGV footprint prediction

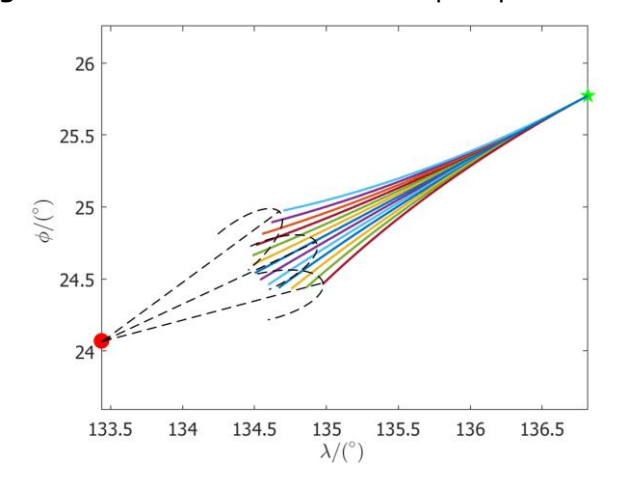


Fig 6. Coverage optimization results of offensive and defensive footprint

Fig. 6 illustrates the coverage of the offensive and defensive footprints. It can be observed from the figure that the three interceptors fully utilize their footprints to completely cover all endpoints of the HBGV's trajectory footprint, verifying the effectiveness of the interception decision-making method.

Furthermore, an interception simulation is conducted based on the multi-interceptor decision-making. Specifically, the midcourse guidance phase of the interceptors adopts pure proportional navigation for deviation correction, while the terminal guidance phase employs kinetic kill technology and a direct force control algorithm based on proportional navigation to regulate the on-off state of the attitude control engine.

Fig. 7 illustrates the 3D offensive-defensive trajectory curves. The actual trajectory of HBGV lies within the maneuverable footprint of interceptor 1; thus, interceptor 1 can successfully intercept the HBGV, with a terminal zero-effort miss (ZEM) of 5.97 m. In contrast, the actual trajectory of the HBGV is at the boundary of the footprints of interceptors 2 and 3. These two interceptors fail to achieve effective deviation correction, resulting in a relatively large miss distance.

The simulation results verify that the proposed multi-interceptor decision-making method can ensure the successful interception of the target by at least one interceptor.

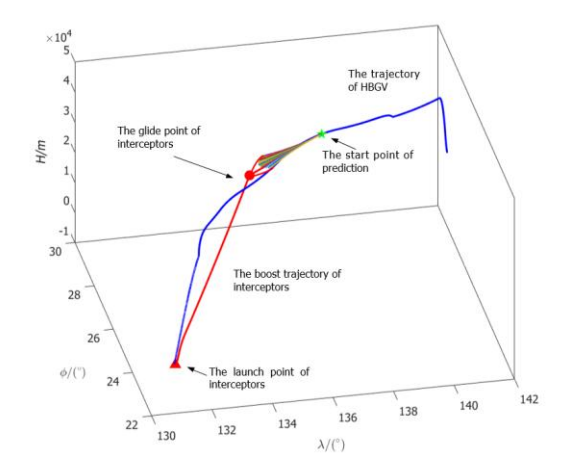


Fig 7. Coverage optimization results of offensive and defensive footprint

#### 6. Conclusion

For the interception of high-speed maneuvering targets within the atmosphere, this paper proposes a multi-interceptor deployment strategy based on rapid footprint prediction and coverage optimization. Specifically, the hypersonic boost-glide vehicle (HBGV) footprint is predicted using a fast computational method, while a mathematical model of the interceptor's maneuverability footprint is established through analysis of its kinematic capabilities. Building on these components, the multi-interceptor deployment problem is transformed into a coverage optimization problem between footprints of HBGV and interceptors . An optimization algorithm is designed to determine a deployment strategy that maximizes coverage of the threat footprint using the minimum number of interceptors. Numerical simulations confirm the effectiveness of the proposed approach, demonstrating its capability to support successful interception with high operational efficiency.

#### References

- 1. 何译宁, 王俊伟, 黄玉薇: 2024年国外高超声速技术领域发展综述. 战术导弹技术(02), 32-43 (2025)
  - He, Y., Wang, J., Huang, Y.: Review of foreign hypersonic technology developments in 2024. Tactical Missile Technology(02), 32-43 (2025)
- 2. Liu, S., Yan, B., Huang, W., Zhang, X., Yan, J.: Current status and prospects of terminal guidance laws for intercepting hypersonic vehicles in near space: a review. J ZHEJIANG UNIV-SC A, 24(5), 387-403 (2023). doi: 10.1631/jzus.A2200423
- 3. Sziroczak, D., Smith, H.: A review of design issues specific to hypersonic flight vehicles. PROG AEROSP SCI, 84, 1-28 (2016)
- 4. 朱一凡, 张学斌, 王维平, 杨峰: 反导防空导弹拦截决策分析模型. 国防科技大学学报(01) (1999)
  - Zhu, Y., Wang, W., Zhang, X., Yang, F.: Analytical Model on Intercepting Decision of Anti<sub>7</sub> Tactical Ballistic Missile. Journal of national university of defense technology(01) (1999)
- 5. 于大腾, 王华, 李林森, 王洪宇: 能量约束下的动能拦截弹逆轨拦截攻击区建模. 宇航学报, 38(07), 704-713 (2017)
  - Yu, D., Wang, H., Li, L., Wang, H.: Attack Area Modeling of Kinetic Kill Vehicle Head-on Interception with Energy Constraint. Journal of Astronautics, 38(07), 704-713 (2017)
- 6. 王子建: 多目标拦截器协同拦截决策方法研究. 硕士, 哈尔滨工业大学 (2020)
  - Wang, Z.: Research on Decision-Making Method of Multi-Target Interceptor Cooperative Interception. Master's Degree, Harbin Institute of Technology (2020)

- 7. 邹子缘, 陈琪锋: 基于决策树搜索的空间飞行器集群对抗目标分配方法. 航空学报, **43(S1)**, 78-88 (2022)
  - Zou, Z., Chen, Q.: Decision Tree Based Target Assignment for Confrontation of Multiple Space Vehicles. Acta Aeronautica et Astronautica Sinica, 43(S1), 78-88 (2022)
- 8. 王泽辉: 防空武器拦截决策系统关键技术研究. 硕士, 西安电子科技大学 (2022)
  - Wang, Z.: Research on Key Technologies of Air Defense Weapon Interception Decision System. Master's Degree, Xidian University (2022)
- 9. Wang, Z., Xin, Y., Wang, C., Zhao, Y.: Research on Key Technologies of Air Defense Weapon Interception Decision System. Paper presented at the International Conference on Guidance, Navigation and Control, Singapore (2022)
- Su, W., Shin, H., Chen, L., Tsourdos, A.: Cooperative interception strategy for multiple inferior missiles against one highly maneuvering target. AEROSP SCI TECHNOL, 80, 91-100 (2018)
- 11. Su, W., Li, K., Chen, L.: Coverage-based three-dimensional cooperative guidance strategy against highly maneuvering target. AEROSP SCI TECHNOL, 85, 556-566 (2019)
- 12. 肖惟, 于江龙, 董希旺, 李清东, 任章: 过载约束下的大机动目标协同拦截. 航空学报, 41(S1), 184-194 (2020)
  - Xiao, W., Yu, J., Dong, X., Li, Q., Ren, Z.: Cooperative Interception Against Highly Maneuvering Target with Acceleration Constraints. Acta Aeronautica et Astronautica Sinica, 41(S1), 184-194 (2020)
- 13. 吴楠: 助推滑翔飞行器预警探测滤波方法与误差链研究. 博士, 国防科学技术大学 (2015)
  - Wu, N.: Study on Filtering Methods and Error Chain in the Boost Glide Vehicle Warning and Detection. Doctor's degree, National University of Defense Technology (2015)
- 14. 吴楠, 王锋, 赵敏, 孟凡坤: 高超声速滑翔再入飞行器的可达区快速预测. 国防科技大学学报, 43(01), 1-6 (2021)
  - Wu, N., Wang, F., Zhao, M., Meng, F.: Fast Prediction for Footprint of Hypersonic Glide Reentry Vehicle. Journal of National University of Defense Technology, 43(01), 1-6 (2021)
- 15. 张凯, 熊家军: 滑翔式高超声速目标可达区域计算方法. 现代防御技术, 45(02), 67-73 (2017) Zhang, K., Xiong, J.: Algorithm of Footprint Area for Gliding Hypersonic Target. Modern Defence Technology, 45(02), 67-73 (2017)
- 16. 阮春荣: 大气中飞行的最优轨迹. 中国宇航出版社, 北京. (1987)
  - Vinh, N.X.: Optimal Trajectories in Atmospheric Flight. Astronautic Publishing House, Beijing. (1987)
- 17. 陈克俊, 刘鲁华, 孟云鹤: 远程火箭飞行动力学与制导. 国防工业出版社. (2014)
  - Chen, K., Liu, L., Meng, Y.: Launch Vehicle Flight Dynamics and Guidance. National Defense Industry Press. (2014)
- 18. 刘思彤, 张占月, 刘达, 许益乔: 高超声速飞行器防御体系建设顶层构想. 现代防御技术, 50(04), 10-16 (2022)
  - Liu, S., Zhang, Z., Liu, D., Xu, Y.: Top-Level Conception of Hypersonic Vehicle Defense System Construction. Modern Defence Technology, **5**0(04), 10-16 (2022)
- 19. 田傲, 曹学伟: 美国高超声速武器防御系统进展分析. 飞航导弹(05), 21-25 (2021)
  - Tian, A., Cao, X.: Progress Analysis of U. S. Hypersonic Weapon Defense System. Aerodynamic Missile Journal (05), 21-25 (2021)